PNAS RESEARCH ARTICLE | PHYSICS

Identification of a nematic pair density wave state in $Bi_2Sr_2CaCu_2O_{8+x}$

Weijiong Chen[a,1], Wangping Ren[a,1], Niall Kennedy[a,b], M. H. Hamidian[c], S. Uchida[d], H. Eisaki[d], Peter D. Johnson[a,e], Shane M. O'Mahony[b], and J. C. Séamus Davis[a,b,c,f]

Contributed by J. C. Séamus Davis; received April 15, 2022; accepted June 23, 2022; reviewed by Hai-Hu Wen and Mats Granath

Electron-pair density wave (PDW) states are now an intense focus of research in the field of cuprate correlated superconductivity. PDWs exhibit periodically modulating superconductive electron pairing that can be visualized directly using scanned Josephson tunneling microscopy (SJTM). Although from theory, intertwining the *d*-wave superconducting (DSC) and PDW order parameters allows a plethora of global electron-pair orders to appear, which one actually occurs in the various cuprates is unknown. Here, we use SJTM to visualize the interplay of PDW and DSC states in $Bi_2Sr_2CaCu_2O_{8+x}$ at a carrier density where the charge density wave modulations are virtually nonexistent. Simultaneous visualization of their amplitudes reveals that the intertwined PDW and DSC are mutually attractive states. Then, by separately imaging the electron-pair density modulations of the two orthogonal PDWs, we discover a robust nematic PDW state. Its spatial arrangement entails Ising domains of opposite nematicity, each consisting primarily of unidirectional and lattice commensurate electron-pair density modulations. Further, we demonstrate by direct imaging that the scattering resonances identifying Zn impurity atom sites occur predominantly within boundaries between these domains. This implies that the nematic PDW state is pinned by Zn atoms, as was recently proposed [Lozano *et al.*, *Phys. Rev. B* 103, L020502 (2021)]. Taken in combination, these data indicate that the PDW in $Bi_2Sr_2CaCu_2O_{8+x}$ is a vestigial nematic pair density wave state [Agterberg *et al. Phys. Rev. B* 91, 054502 (2015); Wardh and Granath arXiv:2203.08250].

cuprate | nematic | pair density wave | vestigial | zinc impurity atom

Significance

Although compelling evidence now exists that a pair density wave (PDW) state occurs in hole-doped CuO_2 materials, its microscopic phenomenology and mechanism remain a mystery. A prevalent theoretical concept has been that the two-dimensional strongly correlated electrons in these materials can spontaneously generate a unidirectional, lattice-commensurate (striped) PDW state that is not induced by any preexistent charge density wave order. Here, in samples with virtually no charge density wave phenomenology, we show by direct scanned Josephson tunneling microscopy visualization of the modulating electron pair density that the PDW state in $Bi_2Sr_2CaCu_2O_{8+x}$ is a vestigial nematic phase, with impurity-atom pinned Ising domains of strongly unidirectional and commensurate pair density modulations.

The existence and phenomenology of PDW states are fundamental issues within the challenge to understand cuprate correlated superconductivity (1–4). Their definitive characteristic is a periodically modulating electron-pair density which can now be visualized directly at the atomic scale, by using scanned Josephson tunneling microscopy (5–9) (SJTM). This new capability allows one to explore both the microscopic electronic structure of the cuprate pair density wave (PDW) state and the interactions between it and the other electronic orders. Understanding the latter is essential, because intertwining the *d*-wave superconducting (DSC) and PDW order parameters allows a plethora of distinct electron-pair orders to appear (1–3), but which one actually occurs in the various cuprates is unknown.

The simplest quantum condensates of electron pairs are defined by a homogeneous superconductive order-parameter

$$\Delta_0(\boldsymbol{r}) = \Delta_0 e^{i\phi(\boldsymbol{r})} \quad [1]$$

for which $\phi(r)$ is the electromagnetic gauge symmetry breaking macroscopic quantum phase. Heuristically, one may think of $\Delta_0 \equiv \sum_k \gamma c_{k\uparrow} c_{-k\downarrow}$, where $c_{k\uparrow}$; $c_{-k\downarrow}$ are electron annihilation operators of opposite spin and momentum and γ the pairing strength, as the amplitude of the electron-pair condensate wavefunction. A unidirectional PDW state is also a superconductor, but one that modulates the condensate order parameter spatially at wavevector P_x such that

$$\Delta_x(\boldsymbol{r}) = \Delta_{P_x}(\boldsymbol{r}) e^{iP_x x} + \Delta_{-P_x}(\boldsymbol{r}) e^{-iP_x x}. \quad [2]$$

In a tetragonal crystal, an orthogonal PDW state can also exist modulating with at wavevector P_y along the *y*-direction as

$$\Delta_y(\boldsymbol{r}) = \Delta_{P_y}(\boldsymbol{r}) e^{iP_y y} + \Delta_{-P_y}(\boldsymbol{r}) e^{-iP_y y}. \quad [3]$$

Because there are then five complex-valued scalar order parameter functions, when these three macroscopic quantum phases are intertwined, a plethora of global electron-pair order parameters becomes possible (1–3, 10–12).

Author contributions: W.C. and J.C.S.D. designed research; M.H.H., S.U., H.E., and J.C.S.D. performed research; W.C., W.R., N.K., P.D.J., and S.O. M. analyzed data; and W.C. and J.C.S.D. wrote the paper.

Reviewers: H.-H.W., Nanjing University; and M.G., University of Gotenburg.

The authors declare no competing interest.

[1]W.C. and W.R. contributed equally to this work.

[2]To whom correspondence may be addressed. Email: jcseamusdavis@gmail.com.

This article contains supporting information online at http://www.pnas.org/lookup/suppl/doi:10.1073/pnas.2206481119/-/DCSupplemental.

Published July 27, 2022.

Theoretical analysis of how the DSC and two primary PDW states become intertwined requires an intricate Ginzburg–Landau–Wilson (GLW) free energy density functional (1–3, 10). Using such an approach, excellent success has been achieved in understanding the induced order parameters, the most prominent of which are the induced charge density wave (CDW) states with order parameters (2, 3) $\rho_{P_x,P_y}(\boldsymbol{r})\propto\Delta_0^*\Delta_{P_x,P_y}+\Delta^*_{-P_x,-P_y}\Delta_0$ and $\rho_{2P_x,2P_y}(\boldsymbol{r})\propto\Delta^*_{-P_x,-P_y}\Delta_{P_x,P_y}$. However, to fully understand the PDW of cuprates, one is not limited to studying such secondary or induced states, because SJTM imaging can give direct access (5–9) to the primary electron-pair orders. The structure and intertwining between PDW and DSC states are described by a subset of terms from the overall GLW free energy density

$$\begin{aligned}\mathcal{F}=&\beta_{c1}|\Delta_0|^2(|\Delta_{P_x}|^2+|\Delta_{P_y}|^2+|\Delta_{P_{-x}}|^2+|\Delta_{P_{-y}}|^2)\\&+\beta_{c2}[\Delta_0^2(\Delta_{P_x}\Delta_{-P_x}+\Delta_{P_y}\Delta_{-P_y})^*\\&+(\Delta_0^2)^*(\Delta_{P_x}\Delta_{-P_x}+\Delta_{P_y}\Delta_{-P_y})],\end{aligned}\qquad[4]$$

where only the lowest order coupling terms are considered and the gradient terms are ignored. Among the possible global electron-pair orders are (2, 3) unidirectional or bidirectional modulated PDW phases $e^{iP_xx};e^{iP_yy}$ with fixed amplitude, as in the Fulde–Ferrell (13) state; and unidirectional or bidirectional modulated PDW amplitudes $|\Delta_{P_x}|cos(P_xx);|\Delta_{P_y}|cos(P_yy)$ with fixed phase, as in the Larkin–Ovchinnikov (14) state. An intriguing hypothetical state has been a nematic pair density wave (2, 3) with order parameter

$$N\equiv(|\Delta_{P_x}|^2+|\Delta_{-P_x}|^2)-(|\Delta_{P_y}|^2+|\Delta_{-P_y}|^2)\qquad[5]$$

and such states may also exhibit vestigial nematic phases (15, 16). But how the DSC and PDW orders are intertwined in cuprates, and their consequent global electron-pair order parameter, are all unknown.

SJTM

Our objective is exploration of intertwined PDW and DSC states in cuprates, by using SJTM. In principle, the total electron-pair density at location $\boldsymbol{r}$, $n(\boldsymbol{r})$, can be visualized by measuring electron-pair (Josephson) critical-current $I_J(\boldsymbol{r})$ from the sample to a superconducting scanning tunneling microscope (STM) tip (17). This is because $n(\boldsymbol{r})\propto I_J^2(\boldsymbol{r})R_N^2(\boldsymbol{r})$, where R_N is the normal-state junction resistance (18, 19). However, since typical thermal fluctuations far exceed the Josephson energy E_J between SJTM tip and sample surface, a phase-diffusive steady-state at voltage V_J drives an electron-pair current $I_P(V_J)=\frac{1}{2}I_J^2ZV_J/(V_J^2+V_c^2)$. Here $V_c=2eZk_BT/\hbar$ with Z the high-frequency impedance of the junction (20, 21). In the theory of such spectra, the maximum value of electron-pair current $I_m=(\hbar/8ek_BT)I_J^2$, providing the basis for atomically resolved SJTM visualization of the electron-pair condensate in superconductors (5–9) as

$$n(\boldsymbol{r})\propto I_m(\boldsymbol{r})\ R_N^2(\boldsymbol{r}).\qquad[6]$$

In that context, we study single crystals of $Bi_2Sr_2CaCu_2O_{8+x}$ with CuO_2 plaquette hole-density $p\approx0.17$, by using a dilution refrigerator based SJTM (5). The cryogenically cleaved samples terminate at the BiO crystal layer, and the d-wave superconducting scan-tip is prepared by exfoliating a nanometer-scale $Bi_2Sr_2CaCu_2O_{8+x}$ flake from that sample surface (5, 9). A typical topographic image at T = 45 mK then consists of atomically resolved and registered surface Bi atoms (Fig. 1*A*) with the typical measured $I_P(V_J)$ shown as an inset. Using such tips and a virtually constant $R_N(\boldsymbol{r})\approx20$ MΩ as determined from analysis of topography at the setup voltage, we image $I_P(V_J,\boldsymbol{r})$ and thus $I_m(\boldsymbol{r})$, at $T=45\ mK$. The Fourier transform of the measured $I_m(\boldsymbol{r})$ image, $I_m(\boldsymbol{q})$, is shown in Fig. 1*B*. In such experiments on $Bi_2Sr_2CaCu_2O_{8+x}$, the $I_m(\boldsymbol{r})$ and $I_m(\boldsymbol{q})$ are both dominated by effects of the crystal supermodulation, a bulk 26-Å periodic modulation of unit-cell dimensions (22) whose general effects are discussed elsewhere (9). The focus of interest here is on the two PDWs observable in $I_m(\boldsymbol{q})$ as four relatively broad peaks surrounding the wavevectors (5) $\boldsymbol{q}\approx\left(\frac{2\pi}{a}\right)(0,\pm0.25);\left(\frac{2\pi}{a}\right)(\pm0.25,0)$. Additionally, the somewhat heterogeneous electron-pair density of the DSC state is represented by the broad peak at $\boldsymbol{q}=\left(\frac{2\pi}{a}\right)(0,0)$. The phenomena detected separately at these five wavevectors can reveal key information on the interplay of the five order parameter functions of Eqs. **1**–**3**.

Interplay of Superconductive and PDW Orders

To separately visualize the two PDWs we inverse Fourier transform $I_m(\boldsymbol{q})$ in Fig. 1*B* for wavevectors $\pm\boldsymbol{P_x}\approx\left(\frac{2\pi}{a}\right)(0,\pm0.25)$ and $\pm\boldsymbol{P_y}\approx\left(\frac{2\pi}{a}\right)(\pm0.25,0)$ respectively, using the $\boldsymbol{q}$-space regions represented inside the colored circles. The resulting $I_{m_x}(\boldsymbol{r})$ and $I_{m_y}(\boldsymbol{r})$ images shown in Fig. 1 *C* and *D*, respectively, reveal the spatial arrangements of the two orthogonal PDW states (in the presence of a predominant DSC.) They are relatively coherent $4a_0$-periodioc modulations with amplitudes differently disordered, and without obvious correlation between them. Clearly, there is a proliferation of edge-dislocation 2π topological defects (23) in $I_{m_{x,y}}(\boldsymbol{r})$, whose ongoing study will be reported elsewhere. Here we concentrate on the interplay of between the simultaneously observed PDW and DSC states.

To do so, we parameterize the two PDW state signatures in terms

$$\begin{aligned}I_{mx,y}(\boldsymbol{r})&=A_{x,y}(\boldsymbol{r})\ cos\left(\boldsymbol{P_{x,y}}\cdot\boldsymbol{r}+\delta_{x,y}(\boldsymbol{r})\right)\\&\equiv\ A_{x,y}(\boldsymbol{r})\ cos\left(\Phi_{\boldsymbol{x,y}}(\boldsymbol{r})\right).\end{aligned}\qquad[7]$$

Fourier component selection at $\pm\boldsymbol{P_x}=\left(\frac{2\pi}{a}\right)(0,\pm0.25)$ and $\pm\boldsymbol{P_y}=\left(\frac{2\pi}{a}\right)(\pm0.25,0)$ then yields

$$I'_m(\boldsymbol{r})\ ==\frac{1}{\sqrt{2\pi}\sigma}\int d\boldsymbol{r}'I_m(\boldsymbol{r}')\ e^{-i\boldsymbol{P_{x,y}}\cdot\boldsymbol{r}'}e^{\frac{|\boldsymbol{r}-\boldsymbol{r}'|^2}{2\sigma_0^2}}\qquad[8]$$

such that

$$A_{x,y}(\boldsymbol{r})\equiv2\sqrt{\left(\mathcal{R}e\ I'_m(\boldsymbol{r})\right)^2+\left(\mathcal{I}m\ I'_m(\boldsymbol{r})\right)^2}\qquad[9]$$

(*SI Appendix*, section 1). The DSC state characteristic, $A_0(\boldsymbol{r})$, is defined similarly by inverse Fourier transform within the yellow circle surrounding wavevector $\boldsymbol{q}=(0,0)$. Identical values of $\sigma_0=\sigma_x=\sigma_y=3$ nm are applied throughout. Using this approach, Fig. 2 *A*–*C* respectively show $A_x(\boldsymbol{r})$, $A_y(\boldsymbol{r})$ and $A_0(\boldsymbol{r})$ visualized simultaneously in the field of view (FOV) of Fig. 1*A*. Thus, it becomes possible to directly explore the phenomenology of intertwining the DSC and PDW states (*SI Appendix*, Section 2). Fig. 2*D* presents measured $\langle A_x+A_y\rangle$ versus A_0, where the average is carried out over all locations $\boldsymbol{r}$ at which $A_0(\boldsymbol{r})$ has the value indicated on the abscissa. The positive slope $s=0.0389$ through zero indicates that, throughout the variations in $A_x(\boldsymbol{r})$, $A_y(\boldsymbol{r})$ and $A_0(\boldsymbol{r})$(Figs. 1 *C* and *D* and 2 *A*–*C*),

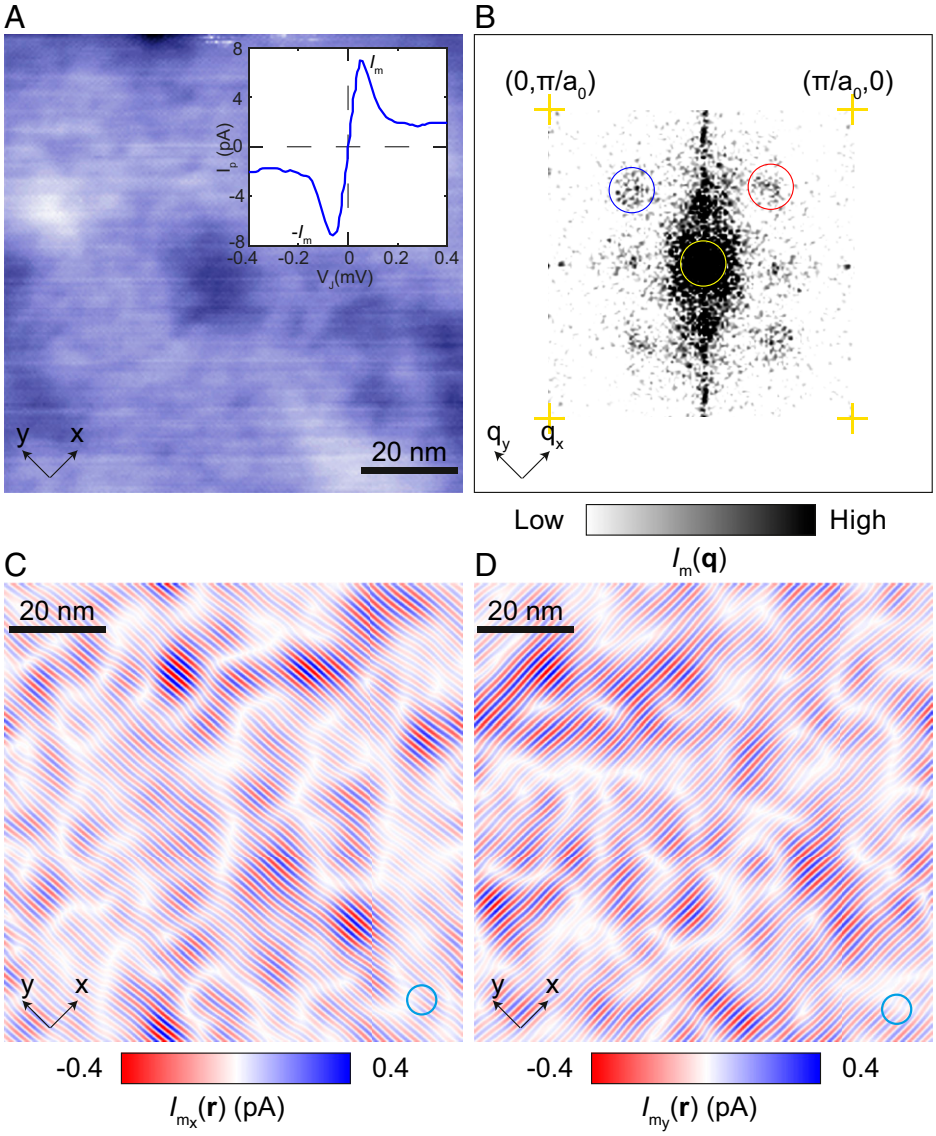

Fig. 1. Visualizing electron pair density $n(\boldsymbol{r})$. (*A*) SJTM topographic image T($\boldsymbol{r}$) of BiO termination layer of $Bi_2Sr_2CaCu_2O_{8+x}$. (*Inset*) Average electron-pair current spectrum $I_P(V_J)$ measured in this FOV at $T = 45\ mK$ and $R_N \approx 20$ MOhm, with maxima occurring at $\pm I_m$. (*B*) Power spectral density Fourier transform of $I_m(\boldsymbol{r})$, $I_m(\boldsymbol{q})$, as measured in FOV of *A*. Four broad PDW peaks surround the wavevectors $\boldsymbol{P} = (2\pi/a)(0, \pm 0.25); (2\pi/a)(\pm 0.25, 0)$ as indicated by pairs of red and blue circles respectively. The DSC electron-pair density is represented by the broad peak at $\boldsymbol{q} = (2\pi/a)(0,0)$ as indicated by the yellow circle. (*C*) Fourier filtration of $I_m(\boldsymbol{q})$ $\boldsymbol{P} = (2\pi/a)(0, \pm 0.25)$ as in *B*, to visualize the $\pm \boldsymbol{P_x}$ PDW modulating along the CuO_2 *x* axis. (*D*) Fourier filtration of $I_m(\boldsymbol{q})$ $\boldsymbol{P} = (2\pi/a)(\pm 0.25, 0)$ in *B*, to visualize the $\pm \boldsymbol{P_y}$ PDW modulating along the CuO_2 *y* axis.

the PDW and the DSC states are mutually enhancing on the average. This conclusion is independent of any inadvertent heterogeneity in the normal-state Josephson junction resistance $R_N(\mathbf{r})$ in Eq. **6**, because it gets divided out by the definition of *s*. The implication of Fig. 2 is that, within the GLW context (Eq. **4** and refs. 1–3), the DSC and PDW states are attractive ($(\beta_{c1} - |\beta_{c2}| < 0)$ electronic phases (*SI Appendix*, section 4) at zero magnetic field, although there is evidence of repulsion when strong gradients are present as in the vortex core.

Discovery of Nematic PDW State in $Bi_2Sr_2CaCu_2O_{8+x}$

Next, to search for the hypothetical (2, 3) nematic PDW state we define a nematic order parameter

$$\mathcal{N}(\boldsymbol{r}) = \{A_x(\boldsymbol{r}) - A_y(\boldsymbol{r})\}/\{A_x(\boldsymbol{r}) + A_y(\boldsymbol{r})\}. \qquad [10]$$

Analyzing the data from Fig. 2 *A* and *B* in this way generates $\mathcal{N}(\mathbf{r})$ as shown in Fig. 3*A*. Again, we note that Eq. **10** provides an empirical definition for a nematic PDW state based directly on $I_m(\boldsymbol{r})$ data, i.e., independent of any possible variations in $R_N(\boldsymbol{r})$. Fig. 3*A* then reveals the existence of strong PDW nematicity in $Bi_2Sr_2CaCu_2O_{8+x}$. Indeed, the histogram of all $\mathcal{N}(\boldsymbol{r})$ values from Fig. 3*A*, *Inset* demonstrates that $|\mathcal{N}(\boldsymbol{r})| > 0.3$ for 45% of the sample area and thus that these nematic PDW states can predominate. To exemplify, Fig. 3*B* shows examples of measured $I_m(\mathbf{r})$ along the *x* axis (*y* axis) in its left (right) panels, both within domains where $\mathcal{N}(\boldsymbol{r}) \gg 0$. Fig. 3*C* shows equivalent exemplary data for domains where $\mathcal{N}(r) \ll 0$. Overall, we find that a robust nematic PDW state, consisting of nanoscale domains of opposite nematicity in electron-pair density, occurs in $Bi_2Sr_2CaCu_2O_{8+x}$ at $p \approx 0.17$.

But this discovery begs the question of what it is that sets the size and location of the nematic PDW domains. One clue comes from recent reports (24) that, in $La_{2-x}Ba_xCuO_4$ away from $p \approx 0.125$, introducing Zn atom substitution at 1% of Cu sites leads to a cascade transition from two-dimensional (2D) superconductivity to three-dimensional superconductivity with falling

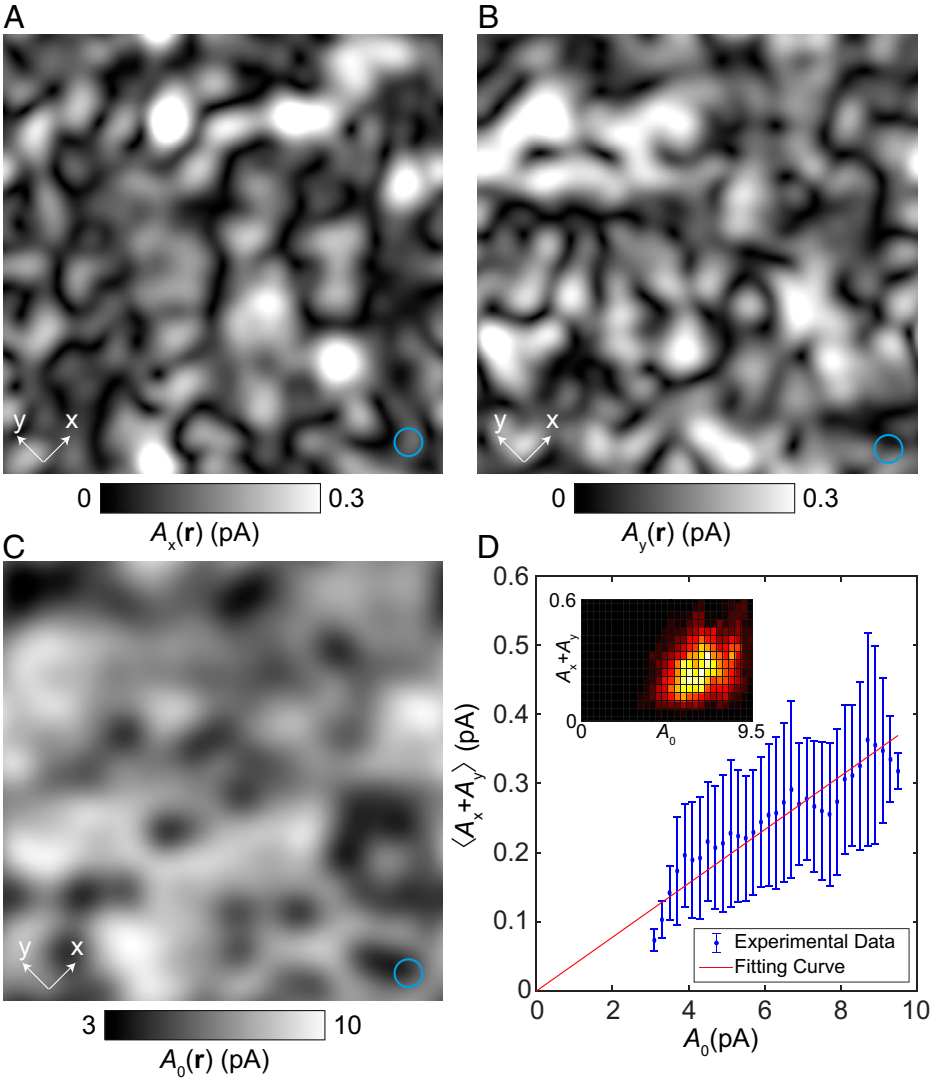

Fig. 2. Intertwined DSC and PDW order parameters. (*A*) Amplitude of $I_m(\boldsymbol{r})$ modulations $A_x(\boldsymbol{r})$ for PDW state with $\pm \boldsymbol{P_x}$, from Fig. 1*C*. (*B*) Amplitude of $I_m(\boldsymbol{r})$ modulations $A_y(\boldsymbol{r})$ for PDW state with $\pm \boldsymbol{P_y}$, from Fig. 1*D*. (*C*) Amplitude of DSC electron-pair density $A_0(\boldsymbol{r})$ derived from Eq. **6** with $\boldsymbol{q} = 0$ as indicated by the yellow circle in Fig. 1*B*. (*D*) $\langle A_x(\boldsymbol{r}) + A_y(\boldsymbol{r}) \rangle$ averaged over all locations $\boldsymbol{r}$ where $A_0(\boldsymbol{r})$ equals the abscissa value A_0. The solid line is a linear fit to these data through (0,0). (*Inset*) The 2D histogram of the same data.

temperature. The inference derived from these studies is that the Zn atoms pins PDW order locally. In cuprates, at each Zn impurity atom there is a superconductive impurity state with energy $E \approx -1$ meV, and also a powerful suppression of electron-pair condensate $n(\boldsymbol{r})$ as exemplified by *SI Appendix*, Fig. S2*F*. In $Bi_2Sr_2CaCu_2O_{8+x}$ the Zn impurity states can be imaged directly in superconducting-tip differential conductance imaging, by finding the local maxima in $Z(\boldsymbol{r}) \equiv \mathrm{I}(20\,\mathrm{mV}, \boldsymbol{r}) - \mathrm{I}(-20\,\mathrm{mV}, \boldsymbol{r})$, where $\mathrm{I}(\mathrm{V})$ is the superconductor–insulator–superconductor single-electron tunnel current. These maxima occur because the coherence peaks of SJTM tip density-of-states near $E \approx \pm 20$ meV are convoluted with the Zn impurity state density-of-states peak $E \approx -1$ meV to produce a strong jump in tunnel currents $\mathrm{I}(E \approx \pm 20\,\mathrm{meV}, \boldsymbol{r})$. Fig. 4*A* shows the resulting image $Z(\boldsymbol{r}) \equiv \mathrm{I}(20\,\mathrm{mV}, \boldsymbol{r}) - \mathrm{I}(-20\,\mathrm{mV}, \boldsymbol{r})$ from which each Zn impurity-state maximum is identified by blue circles (*SI Appendix*, section 3). In Fig. 4*B* we show the amplitude of nematic order parameter $|\mathcal{N}(\boldsymbol{r})|$ with the sites of Zn impurity resonances overlaid as blue dots. Visually the Zn sites seem to occur near the domain boundaries in $|\mathcal{N}(\boldsymbol{r})|$. This can be quantified by plotting the histogram of the distribution of distances between each Zn impurity atom and its nearest PDW domain wall and comparing to the expected average distance of uncorrelated random points. The result shown in Fig. 4*C* reveals that the Zn sites occur highly preferentially near the boundaries of the PDW Ising domains. This direct visualization indicates that the PDW nematic domains are pinned by interactions with Zn impurity atoms at the Cu sites and is therefore highly consistent with deductions from the transport studies of Zn-doped $La_{2-x}Ba_xCuO_4$ (24).

Discussion and Conclusion

Spectroscopic imaging STM and resonant X-ray scattering have produced a wealth of understanding of unidirectionality, commensuration and domain formation for CDW modulations in strongly underdoped cuprates. However, because photon scattering cannot (yet) detect PDW states, because the pseudogap in single particle tunneling masks the true electron-pairing energy gap and thus order parameter, and because SJTM visualization of PDW states is recent (5–9), equivalent issues for the cuprate PDW state are unresolved. Our SJTM visualization now demonstrates that the $Bi_2Sr_2CaCu_2O_{8+x}$ PDW states tend strongly to be both unidirectional and commensurate, a situation widely predicted (25–34) as a consequence of strong-coupling physics

within the CuO_2 Hubbard model. Further, we note that visualization of these characteristics in a robust PDW state occurs in $Bi_2Sr_2CaCu_2O_{8+x}$ at a carrier density where the CDW modulations are virtually nonexistent (35, 36), as is the empirical case in the samples studied here (*SI Appendix*, Fig. S3). The implication, consistent with the eight unit-cell periodic energy gap modulations observed in single particle tunneling (37, 38), is that the $Bi_2Sr_2CaCu_2O_{8+x}$ PDW states are not induced by the existence of a CDW and instead are the primary translation symmetry breaking state of hole-doped CuO_2. Furthermore, since the spatial configurations of the PDWs studied here appear uninfluenced by a preexistent CDW yet are obviously disordered, effects of chemical (and possibly dopant-ion) randomness on the PDW are adumbrated. Indeed, recent transport studies (24) provide

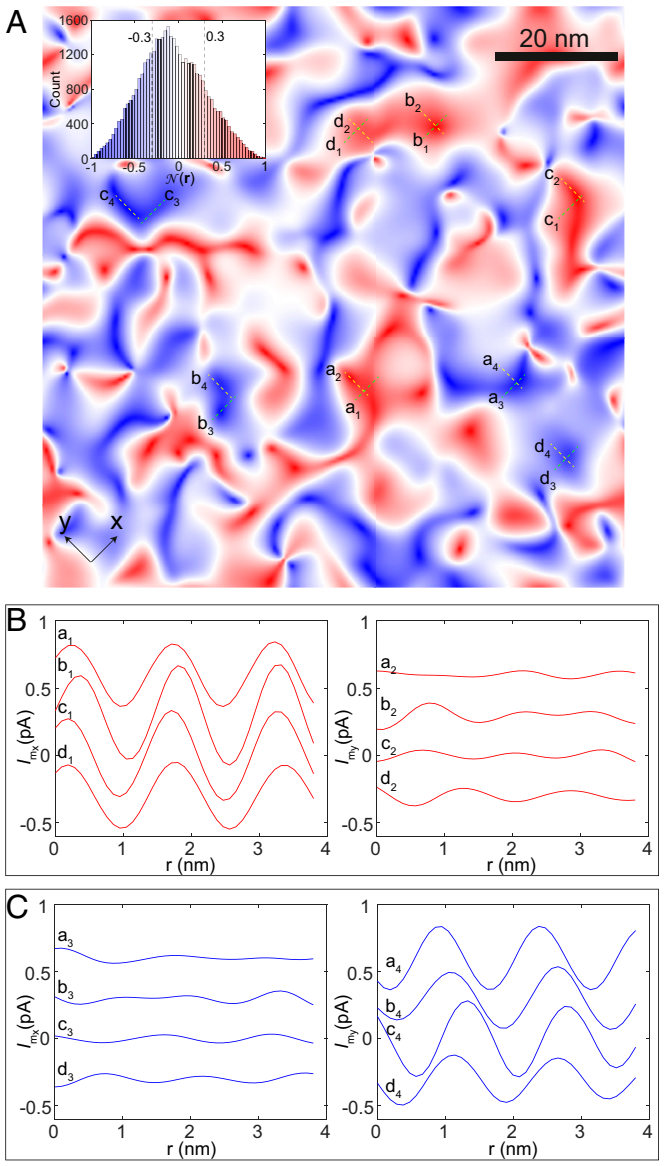

Fig. 3. Nematic PDW State of $Bi_2Sr_2CaCu_2O_{8+x}$. (*A*) Nematic order parameter $\mathcal{N}(\mathbf{r}) = \{A_x(\mathbf{r}) - A_y(\mathbf{r})\}/\{A_x(\mathbf{r}) + A_y(\mathbf{r})\}$ derived from Fig. 2 *A* and *B*. Domains of opposite nematicity occur with correlation length $\xi \approx 15$nm. (*Inset*) Histogram of all $\mathcal{N}(\mathbf{r})$ values in *A*, showing nonzero mean value. The magnitude $|\mathcal{N}| > 0.3$ for approximately 45% of the FOV, indicating a strong nematic interaction between the two PDW. (*B*, *Left*) Four examples of measured $I_m(\mathbf{r})$ along the *x* axis. (*B*, *Right*) Four examples of measured $I_m(\mathbf{r})$ along the *y* axis, both within domains where $\mathcal{N}(\mathbf{r}) \gg 0$. (*C*, *Left*) Four examples of measured $I_m(\mathbf{r})$ along the *x* axis. (*C*, *Right*) Four examples of measured $I_m(\mathbf{r})$ along the *y* axis, both within domains where $\mathcal{N}(\mathbf{r}) \ll 0$.

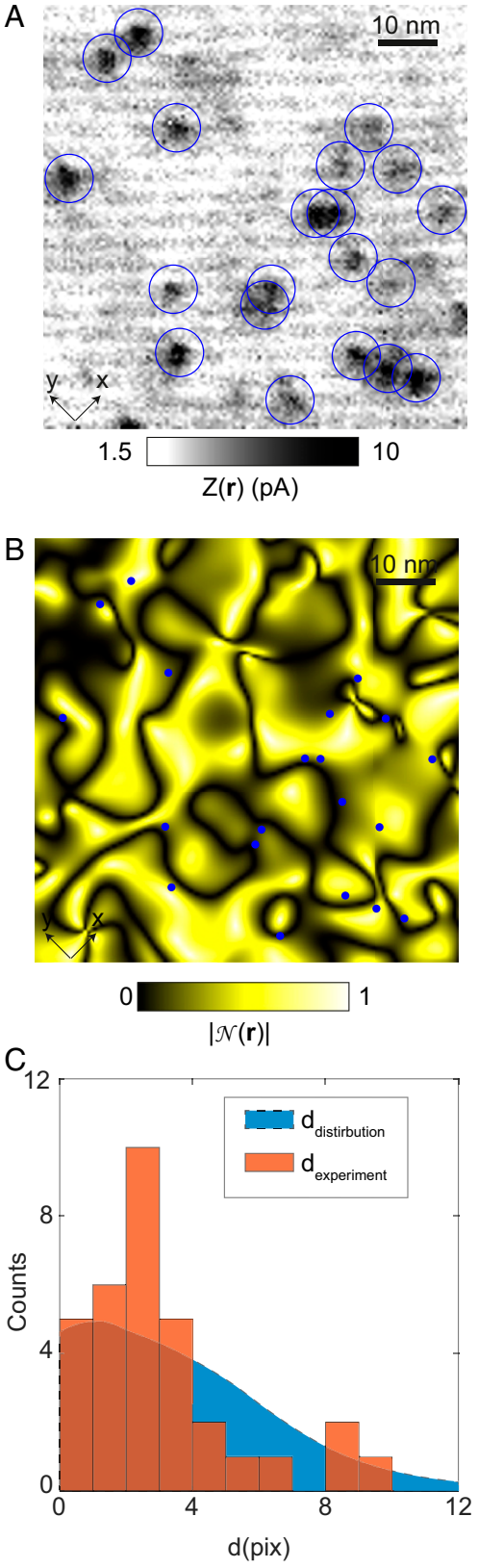

Fig. 4. Pinning of PDW nematic domains by Zn impurity atoms. (*A*) Locations of Zn impurity atoms $Z(\mathbf{r})$ as detected in $Z(r) \equiv I(r, 20\text{ mV}) - I(r, -20\text{ mV})$ are shown as blue circles. The identification and register of Zn impurity sites is discussed in *SI Appendix*, section 3. (*B*) $|\mathcal{N}(\mathbf{r})|$, the amplitude of the nematic order parameter from Fig. 3*A*, with the sites of Zn impurity resonances overlaid as blue dots. (*C*) The distribution of distances between each Zn impurity atoms and its nearest PDW domain walls (red). This is compared to the expected average distance if there is no correlation between Zn impurity atoms and the PDW domain walls (blue). Zn impurity atoms are concentrated near the PDW domain walls.

experimental evidence that Zn impurity atoms pin the PDW order in $La_{2-x}Ba_xCuO_4$. For comparison, our visualization of the $Bi_2Sr_2CaCu_2O_{8+x}$ PDW nematic domains simultaneously with Zn scattering resonances demonstrates directly that the Zn impurity-atom sites occur predominantly within boundary regions between these domains. Overall, a vestigial state is one that only partially breaks the symmetry of the true ordered state. Here we find a nematic PDW state breaking the rotational (C_4) symmetry of the lattice but not long-range translational symmetry, in what appears to be a disorder-pinned realization of a global nematic order. Hence, a plausible context in which to consider the PDW in $Bi_2Sr_2CaCu_2O_{8+x}$ is as a new form of vestigial nematic state based on a disordered unidirectional density wave of electron pairs (39) rather than of single electrons (40).

Ergo, by using SJTM to simultaneously visualize the PDW and DSC states of $Bi_2Sr_2CaCu_2O_{8+x}$ near $p \approx 0.17$ where no CDW phenomena obtrude, we demonstrate that they are intertwined in mutually attractive phases (Fig. 2). Conversely, separate imaging of the electron-pair density modulations of the two orthogonal PDWs reveals a robust nematic PDW state, with primarily unidirectional and lattice-commensurate electron-pair density modulations forming Ising domains of opposite nematicity (Fig. 3). Imaging the sites of Zn impurity-states finds them occurring preferentially in boundary regions of minimal nematic order (Fig. 4), implying that the PDW domains are pinned thereby. Generally, these data signify that the PDW state of $Bi_2Sr_2CaCu_2O_{8+x}$ is a vestigial nematic phase of electron pairs, that it is locally unidirectional and lattice commensurate, and that it is not a subordinate but a primary electronic order of hole-doped CuO_2.

Data Availability. All study data are included in the article and/or *SI Appendix*.

ACKNOWLEDGMENTS. We acknowledge and thank Owen H. S. Davis and Shuqiu Wang for key discussions and suggestions. M.H.H. and J.C.S.D. acknowledge support from the Moore Foundation's EPiQS Initiative through grant GBMF9457. W.R. and J.C.S.D. acknowledge support from the European Research Council under award DLV-788932. W.C. and J.C.S.D. acknowledge support from the Royal Society under award R64897. N.K., S.O., and J.C.S.D. acknowledge support from the Science Foundation of Ireland under award SFI 17/RP/5445. H.E. acknowledges support from Japan Society for the Promotion of Science KAKENHI (no. JP19H05823). P.D.J. acknowledges support by QuantEmX grant GBMF9616 from ICAM/Moore Foundation and by a Visiting Fellowship at Wadham College, Oxford.

Author affiliations: [a]Clarendon Laboratory, University of Oxford, Oxford OX1 3PU, United Kingdom; [b]Department of Physics, University College Cork, Cork T12 R5C, Ireland; [c]Department of Physics, Cornell University, Ithaca, NY 14850; [d]Institute of Advanced Industrial Science and Technology, Ibaraki 305-8568, Japan; [e]Condensed Matter Physics & Materials Science Department, Brookhaven National Laboratory, Upton, NY 11973; and [f]Max Planck Institute for Chemical Physics of Solids, D-01187 Dresden, Germany

1. E. Berg, E. Fradkin, S. A. Kivelson, J. M. Tranquada, Striped superconductors: How spin, charge and superconducting orders intertwine in the cuprates. *New J. Phys.* **11**, 115004 (2009).
2. E. Fradkin, S. A. Kivelson, J. M. Tranquada, Colloquium: Theory of intertwined orders in high temperature superconductors. *Rev. Mod. Phys.* **87**, 457–482 (2015).
3. D. F. Agterberg *et al.*, The physics of pair-density waves: Cuprate superconductors and beyond. *Annu. Rev. Condens. Matter Phys.* **11**, 231–270 (2020).
4. J. M. Tranquada, Cuprate superconductors as viewed through a striped lens. *Adv. Phys.* **69**, 437–509 (2020).
5. M. H. Hamidian *et al.*, Detection of a Cooper-pair density wave in $Bi_2Sr_2CaCu_2O_{8+x}$. *Nature* **532**, 343–347 (2016).
6. D. Cho, K. M. Bastiaans, D. Chatzopoulos, G. D. Gu, M. P. Allan, A strongly inhomogeneous superfluid in an iron-based superconductor. *Nature* **571**, 541–545 (2019).
7. X. Liu, Y. X. Chong, R. Sharma, J. C. Seamus Davis, Discovery of a Cooper-pair density wave state in a transition-metal dichalcogenide. *Science* **372**, 1447–1452 (2021).
8. X. Liu, Y. X. Chong, R. Sharma, J. C. S. Davis, Atomic-scale visualization of electronic fluid flow. *Nat. Mater.* **20**, 1480–1484 (2021).
9. S. M. O'Mahony *et al.*, On the electron pairing mechanism of copper-oxide high temperature superconductivity. arXiv [Preprint] (2022). https://arxiv.org/abs/2108.03655. Accessed 30 January 2022.
10. D. F. Agterberg, H. Tsunetsugu, Dislocations and vortices in pair-density-wave superconductors. *Nat. Phys.* **4**, 639–642 (2008).
11. E. Berg, E. Fradkin, S. A. Kivelson, Charge-4e superconductivity from pair-density- wave order in certain high-temperature superconductors. *Nat. Phys.* **5**, 830 (2009).
12. L. Radzihovsky, A. Vishwanath, Quantum liquid crystals in an imbalanced Fermi gas: Fluctuations and fractional vortices in Larkin-Ovchinnikov states. *Phys. Rev. Lett.* **103**, 010404 (2009).
13. P. Fulde, R. A. Ferrell, Superconductivity in a strong spin-exchange Field. *Phys. Rev.* **135**, A550–A563 (1964).
14. A. I. Larkin, Y. N. Ovchinnikov, Nonuniform state of superconductor. *Zh. Eksp. Teor. Fiz* **47**, 1136 (1964) [translation: *Sov. Phys. JETP* **20**, 762 (1965)].
15. D. F. Agterberg, D. S. Melchert, M. K. Kashyap, Emergent loop current order from pair density wave superconductivity. *Phys. Rev. B* **91**, 054502 (2015).
16. J. Wårdh, M. Granath, Nematic single-component superconductivity and loop-current order from pair-density wave instability. arXiv [Preprint] (2022). https://arxiv.org/abs/2203.08250. Accessed 15 March 2022.
17. S. H. Pan, E. W. Hudson, J. C. Davis, Vacuum tunneling of superconducting quasiparticles from atomically sharp scanning tunneling microscope tips. *Appl. Phys. Lett.* **73**, 2992–2994 (1998).
18. J. Šmakov, I. Martin, A. V. Balatsky, Josephson scanning tunneling microscopy. *Phys. Rev. B* **64**, 212506 (2001).
19. M. Graham, D. K. Morr, Josephson scanning tunneling spectroscopy in d_{x2-y2}-wave superconductors: A probe for the nature of the pseudogap in the cuprate superconductors. *Phys. Rev. Lett.* **123**, 017001 (2019).
20. G.-L. Ingold, H. Grabert, U. Eberhardt, Cooper-pair current through ultrasmall Josephson junctions. *Phys. Rev. B Condens. Matter* **50**, 395–402 (1994).
21. Y. M. I. Anchenko, L. A. Zil'Berman, The Josephson effect in small tunnel contacts. *Soviet J. Exp. Theor. Phys.* **55**, 2395–2402 (1969).
22. Y. Gao, P. Lee, P. Coppens, M. A. Subramania, A. W. Sleight, The incommensurate modulation of the 2212 Bi-Sr-Ca-Cu-O superconductor. *Science* **241**, 954–956 (1988).
23. A. Mesaros *et al.*, Topological defects coupling smectic modulations to intra-unit-cell nematicity in cuprates. *Science* **333**, 426–430 (2011).
24. P. M. Lozano, G. D. Gu, J. M. Tranquada, Q. Li, Experimental evidence that zinc impurities pin pair-density-wave order in $La_{2-x}Ba_xCuO_4$. *Phys. Rev. B* **103**, L020502 (2021).
25. A. Himeda, T. Kato, M. Ogata, Stripe states with spatially oscillating d-wave superconductivity in the two-dimensional t-t'-J model. *Phys. Rev. Lett.* **88**, 117001 (2002).
26. M. Raczkowski *et al.*, Unidirectional *d*-wave superconducting domains in the two-dimensional *t-J* model. *Phys. Rev. B* **76**, 140505 (2007).
27. E. Berg *et al.*, Dynamical layer decoupling in a stripe-ordered high-T_c superconductor. *Phys. Rev. Lett.* **99**, 127003 (2007).
28. K.-Y. Yang, W. Q. Chen, T. M. Rice, M. Sigrist, F.-C. Zhang, Nature of stripes in the generalized t-J model applied to cuprate superconductors. *New J. Phys.* **11**, 055053 (2009).
29. F. Loder, S. Graser, A. P. Kampf, T. Kopp, Mean-field pairing theory for the charge-stripe phase of high-temperature cuprate superconductors. *Phys. Rev. Lett.* **107**, 187001 (2011).
30. P. Corboz, T. M. Rice, M. Troyer, Competing states in the *t-J* model: Uniform *D*-wave state versus stripe state. *Phys. Rev. Lett.* **113**, 046402 (2014).
31. P. Choubey *et al.*, Atomic-scale electronic structure of the cuprate pair density wave state coexisting with superconductivity. *Proc. Natl. Acad. Sci. U.S.A.* **117**, 14805–14811 (2020).
32. S. S. Dash, D. Sénéchal, Charge- and pair-density-wave orders in the one-band Hubbard model with dynamical mean field theory. *Phys. Rev. B* **103**, 045142 (2021).
33. S. Yoshida, K. Yada, Y. Tanaka, Theory of pair density wave on a quasi-one-dimensional lattice in the Hubbard model. *Phys. Rev. B* **104**, 094506 (2021).
34. P. Mai, S. Karakuzu, G. Balduzzi, S. Johnston, T. A. Maier, Intertwined spin, charge, and pair correlations in the two-dimensional Hubbard model in the thermodynamic limit. *Proc. Natl. Acad. Sci. U.S.A.* **119**, e2112806119 (2022).
35. K. Fujita *et al.*, Simultaneous transitions in cuprate momentum-space topology and electronic symmetry breaking. *Science* **344**, 612–616 (2014).
36. R. Arpaia *et al.*, Dynamical charge density fluctuations pervading the phase diagram of a Cu-based high-T_c superconductor. *Science* **365**, 906–910 (2019).
37. S. D. Edkins *et al.*, Magnetic field-induced pair density wave state in the cuprate vortex halo. *Science* **364**, 976–980 (2019).
38. Z. Du *et al.*, Imaging the energy gap modulations of the cuprate pair-density-wave state. *Nature* **580**, 65–70 (2020).
39. J. Wårdh *et al.*, Colossal transverse magnetoresistance due to nematic superconducting phase fluctuations in a copper oxide. arXiv [Preprint] (2022). https://arxiv.org/abs/2203.06769. Accessed 13 March 2022.
40. L. Nie, G. Tarjus, S. A. Kivelson, Quenched disorder and vestigial nematicity in the pseudogap regime of the cuprates. *Proc. Natl. Acad. Sci. U.S.A.* **111**, 7980–7985 (2014).